Mechanical and Durability Performance of Lateritic Clay Soil Stabilized with Bitumen Emulsion and Iron Ore Tailings for Pavement Subbase Construction

S. T. Stevens[1]*, C. Kanali[2], I. Ngassam[3], K. Abongo[1]

[1]Department of Civil Engineering, Pan African University Institute for Basic Sciences, Technology, and Innovation, Nairobi, Kenya.
[2]Department of Agricultural and Biosystems Engineering, Jomo Kenyatta University of Agriculture and Technology, Nairobi, Kenya.
[3]Department of Civil and Architectural Engineering, University of Buea, Buea, Cameroon.

ABSTRACT: Lateritic clay soils, prevalent across tropical sub-Saharan Africa, present significant challenges for pavement construction due to their high plasticity (liquid limit of 56%, plasticity index of 24%) and low bearing capacity (CBR of 18.5%), necessitating stabilisation for subbase use. This study explores a novel stabilisation approach combining cationic bitumen emulsion (K3-65) with iron ore tailings (IOT) to identify an optimal, cost-effective mix for tropical pavement subbase applications. A full factorial experimental design was implemented, testing 16 mix proportions with bitumen emulsion ranging from 2–10% and IOT from 10–30%. Mechanical performance was evaluated at 7, 14, and 28 days through California Bearing Ratio (CBR), Unconfined Compressive Strength (UCS), and Indirect Tensile Strength (ITS) tests, using a total of 432 specimens. Comprehensive durability assessments included wet-dry mass loss, retained UCS (Durability Index), hydraulic conductivity, and moisture susceptibility via the Tensile Strength Ratio (TSR). Material characterisation, Atterberg limits, grain size, XRF, and SEM-EDS were performed on raw materials to elucidate stabilisation mechanisms. Statistical analysis using one-way ANOVA ($\alpha=0.05$) and Tukey's HSD test confirmed that mix proportions significantly influenced all performance metrics ($p<0.001$). The optimal formulation, identified as 4% bitumen emulsion with 20% IOT (Mix M5), achieved substantial improvements over the untreated soil: a 28-day CBR of 28.6% (+55%), UCS of 17.3 MPa (+182%), and ITS of 3.9 MPa. Crucially, this mix uniquely satisfied all durability thresholds, exhibiting a durability index of 88.1%, hydraulic conductivity of 6.4×10^{-6} cm/s, and a TSR of 88.7%, surpassing the AASHTO T283 minimum of 80%. These findings establish the 4% bitumen emulsion + 20% IOT combination as a technically viable, lower-carbon alternative to conventional cement stabilisation. The study recommends this stabilised mix for subbase construction at a compacted thickness of 150–200 mm, with a minimum 14-day curing period before opening to traffic.

***KEYWORDS*:** Bitumen Emulsion, California Bearing Ratio, Durability Index, Iron Ore Tailings, Laterite stabilization, Pavement Subbase, Unconfined Compressive Strength

[Received Apr. 17, 2026; Revised May. 05, 2026; Accepted May. 12, 2026] Print ISSN: 0189-9546 | Online ISSN: 2437-2110

I. INTRODUCTION

Rapid infrastructure expansion in emerging economies across sub-Saharan Africa has intensified demand for durable, cost-effective, and environmentally responsible construction materials (Sharma et al., 2025). Road networks are fundamental to trade, mobility, and access to basic services, yet most rural and peri-urban roads in tropical Africa are built on naturally occurring lateritic soils that frequently exhibit inadequate engineering properties in their untreated state (Junior & Franks, 2022). These soils are characterized by high plasticity, elevated fines content, low bearing capacity, and pronounced moisture sensitivity, all of which contribute to structural distress under traffic loading when used as subbase or subgrade materials without stabilization (Ezreig et al., 2022).

Conventional stabilization methods using ordinary Portland cement (OPC) or hydrated lime have demonstrated consistent effectiveness in improving lateritic soil strength and durability. However, these binders present significant environmental and economic challenges, including high energy consumption during production, elevated carbon footprints, and escalating material costs in remote tropical regions (Dhar & Hussain, 2021). As a result, research attention has shifted toward sustainable alternatives that leverage industrial and mining by-products to enhance soil performance while promoting waste valorisation (Bommi et al., 2025).

Bitumen emulsion stabilization has gained considerable attention for fine-grained soils due to its flexibility, water resistance, and capacity to reduce moisture-induced damage (Sam et al., 2024). Unlike cement-treated soils, bitumen-stabilized materials exhibit improved resistance to fatigue cracking and deformation under cyclic environmental loading (Al-mohammedawi & Mollenhauer, 2022). Simultaneously, iron ore tailings (IOT) generated in large volumes from mining

*Corresponding author: stanleystevens89@gmail.com
doi: http://doi.org/10.63746/njtd.v23i2.4669

operations present significant environmental disposal challenges. Their fine granular structure, high specific gravity, and mineral composition rich in iron oxides give IOT the potential to function as stabilizing additives capable of improving soil density, stiffness, and load-bearing capacity when incorporated into a soil matrix (Babatunde et al., 2020).

Previous studies have investigated bitumen emulsion and IOT independently as soil stabilizers. Bitumen-stabilized soils have shown improved CBR and reduced moisture susceptibility at optimal binder contents of 3–6% (Mizher et al., 2024), while IOT incorporation at 10–30% has enhanced UCS and dry density in fine-grained soils through densification and particle interlocking (Kaze et al., 2021). However, these materials have fundamentally different mechanisms bitumen improves cohesion and moisture resistance while IOT improves stiffness and packing density, and their concurrent application in a combined stabilization framework remains critically underexplored. No published study has systematically evaluated how the competing effects of bitumen-induced cohesion and IOT-induced stiffness interact across a wide range of combined dosages to define an optimum mix for subbase application. The bitumen emulsion range (2–10%) was guided by prior studies demonstrating peak strength improvements at moderate emulsion contents with deterioration beyond 6–8% due to lubrication effects (Al-mohammedawi & Mollenhauer, 2022). The IOT range (10–30%) was adopted following Babatunde et al. (2020) and Bahmani et al. (2025), who reported diminishing returns and increased brittleness beyond 30% IOT addition.

A critical knowledge gap exists in the simultaneous assessment of bitumen emulsion and IOT as a complementary combined system for stabilizing highly plastic lateritic clays (A-7-6). Existing research treats these agents independently and does not address the mechanistic interplay between bitumen-induced flexibility and IOT-induced stiffness, particularly with respect to preventing fatigue cracking, rutting, and moisture softening under combined loading. The novelty of this study lies in the systematic, simultaneous evaluation of bitumen emulsion and IOT across 16 mix proportions and three curing ages, providing the first comprehensive durability envelope combining mass loss, retained strength (Durability Index), hydraulic conductivity, and TSR for IOT-bitumen stabilized laterite in a tropical East African context.

This study examines the mechanical and durability performance of bitumen emulsion and iron ore tailings as a combined stabilization system for AASHTO A-7-6 lateritic clay, to identify an optimum mix for tropical pavement subbase construction.

II. MATERIALS AND METHODS

A. Material Acquisition and Preparation

Three primary materials were used: lateritic clay soil, cationic bitumen emulsion (K3-65), and iron ore tailings (IOT). The lateritic soil was sampled from a borrow pit in Thika, Kiambu County, Kenya, at 0.5–1.0 m depth. Samples were sealed in polyethylene bags, transported to the Transport and Highway Engineering Laboratory, Nairobi, air-dried at 25–30°C for 72 hours, pulverized, and sieved through 4.75 mm. IOT were procured from a mining dump in Taita Taveta County, Kenya (transport distance: approximately 370 km to Thika). Approximately 50 kg was collected from 0.3–0.5 m depth, transported in sealed polypropylene bags, air-dried for 48 hours, and sieved through 4.75 mm. The tailings consist predominantly of quartz, hematite, and goethite particles. The K3-65 slow-setting cationic bitumen emulsion was sourced from the MTRD Bitumen Laboratory, Ministry of Transport and Infrastructure, Nairobi, and stored in sealed 20-litre containers at approximately 25°C away from direct sunlight.

B. Material Characterization

Each material was characterized based on ASTM and BS 1377:1990 standards. Atterberg limits (ASTM D4318), grain size distribution (ASTM D422 + hydrometer), standard Proctor compaction (ASTM D698), specific gravity (ASTM D854), and CBR (ASTM D1883) were determined for the lateritic soil. XRF analysis was conducted for chemical oxide composition of both soil and IOT. AASHTO M145 was used for soil classification.

To verification the Concretionary Nodule Nature of Gravel Fraction, the A-7-6 classification is governed by Atterberg limits (LL > 41%; PI ≥ LL − 30), which the soil satisfies (LL = 56%, PI = 24%), irrespective of gravel content. To provide direct evidence that the high gravel fraction (46.91%) consists of iron-cemented concretionary nodules rather than primary detrital gravel, the following additional characterization was performed. First, Atterberg limits were determined separately on the fraction passing the 425 μm sieve per ASTM D4318. The PI of the <425 μm fraction was determined as $PI_{<425}$ = 28.4% (LL = 59.8%, PL = 31.4%) higher than the whole-soil PI (24%) confirming that the coarse fraction dilutes plasticity and is non-plastic, consistent with inert iron-cemented concretions rather than active clay gravel. Second, scanning electron microscopy (SEM) with Energy Dispersive Spectroscopy (EDS) was performed on representative particles from the gravel fraction (retained on 4.75 mm sieve). SEM imaging revealed an irregular, porous internal structure with crystalline clusters, clearly distinguishing the nodules from primary rounded mineral gravel. EDS analysis confirmed Fe (≈38 at.%) and O (≈42 at.%) dominance, with minor Al, Si, and trace elements, consistent with a goethite and hematite-cemented lateritic concretionary matrix. SEM+EDS micrographs and spectrum are presented in Figure 1. These results confirm that the gravel fraction consists of cemented concretionary aggregates that disaggregate under traffic loading, confirming clay-mineral dominance over engineering behaviour.

C. Mix Design and Experimental Procedures

A full factorial experimental design was adopted comprising five bitumen emulsion levels (0, 2, 4, 6, 8, 10%) × 3 IOT levels (10, 20, 30%), yielding 16 distinct mix proportions (M0–M15) as detailed in Table 1. Each mix was prepared at its corresponding OMC and MDD, compacted into standard moulds, and cured for 7, 14, and 28 days at 25 ± 2°C and relative humidity ≥95%, wrapped in polyethylene sheeting to prevent moisture loss. Three replicate specimens were prepared per mix per curing age (n = 3) per mechanical test, yielding 144 specimens per test (432 total across CBR, UCS, and ITS). All reported values represent the arithmetic mean of three replicates, with standard deviation and coefficient of variation computed for each dataset. Soil was first dry-mixed with the designated IOT proportion until homogeneous; bitumen emulsion was then added incrementally while mixing continuously to ensure uniform particle coating. The blend was compacted at OMC and MDD into standard cylindrical or split-mould specimens as appropriate for each test.

Table 1 Mix Proportions, Compaction Parameters, and Replication Plan

Mix ID	Emulsion (%)	IOT (%)	OMC (%)	MDD (kg/m³)	Replicates	Curing Ages (days)
M0 (Control)	0	0	18.5	1565	3	7, 14, 28
M1	2	10	17.2	1589	3	7, 14, 28
M2	2	20	17.5	1602	3	7, 14, 28
M3	2	30	17.8	1615	3	7, 14, 28
M4	4	10	16.8	1624	3	7, 14, 28
M5	4	20	17.0	1641	3	7, 14, 28
M6	4	30	17.3	1635	3	7, 14, 28
M7	6	10	16.5	1618	3	7, 14, 28
M8	6	20	16.7	1622	3	7, 14, 28
M9	6	30	17.0	1610	3	7, 14, 28
M10	8	10	16.2	1598	3	7, 14, 28
M11	8	20	16.4	1605	3	7, 14, 28
M12	8	30	16.8	1595	3	7, 14, 28
M13	10	10	16.0	1572	3	7, 14, 28
M14	10	20	16.2	1580	3	7, 14, 28
M15	10	30	16.5	1565	3	7, 14, 28

MDD = Maximum Dry Density (kg/m³); OMC = Optimum Moisture Content. Curing: 25 ± 2°C, ≥95% RH. n = 3 per test per mix per curing age; total specimens = 432 across CBR, UCS, and ITS.

D. Mechanical Testing

Three mechanical performance tests were conducted at each curing age. (i) California Bearing Ratio (CBR): Conducted per ASTM D1883/AASHTO T193 on soaked specimens. (ii) Unconfined Compressive Strength (UCS): Conducted per ASTM D2166. All UCS specimens were cylindrical, 50 mm internal diameter × 100 mm height (H:D = 2:1 per ASTM D2166). Specimen dimensions were verified to ±1 mm by calibrated vernier calliper before testing; specimens deviating beyond this tolerance were discarded. Specimen ends were trimmed flat using a steel wire saw to remove compaction surface irregularities. No Sulphur capping was applied; thin rubber membrane pads (3 mm) were placed at both platen–specimen interfaces to distribute applied stress uniformly, eliminating contact stress concentrations per standard ASTM D2166 practice for compacted stabilized soils. Axial load was applied at a constant strain rate of 1.0%/min (equivalent to 1.0 mm/min for the 100 mm specimen height) per ASTM D2166. Testing temperature was maintained at 20–22°C. Load and axial deformation were recorded continuously at 0.1 mm intervals throughout each test. Failure was identified at the peak load or at 20% axial strain, whichever occurred first. Failure strains at peak load were recorded for all specimens and are reported for M0, M5, and M15 in Table 2 and discussed in Section III.B. Stress–strain curves for M0 (control), M5 (optimum), and M15 (over-stabilized) at 28-day curing are presented in Figure 12. (iii) Indirect Tensile Strength (ITS): Conducted per ASTM D6931 on compacted cylindrical specimens. ITS evaluates tensile resistance and crack propagation potential, critical for fatigue performance of pavement layers under repeated traffic loading.

E. Durability Testing

Three durability protocols were employed to simulate the tropical environmental exposure. (i) Wet-Dry Cycle Testing**:** Per ASTM D559 using 12 wetting–drying cycles (5 h wetting at 23°C + 42 h oven-drying at 71°C). Mass loss (%) was recorded after all 12 cycles. In addition, retained UCS was determined on three replicate specimens per selected mix after completion of the full 12-cycle protocol. The Durability Index (DI) was computed as $DI = (UCS_{post} / UCS_{pre}) \times 100$ (%), where UCS_{post} is the mean UCS after 12 wet-dry cycles and UCS_{pre} is the mean 28-day UCS before cycling. A DI ≥ 80% is adopted as the acceptance criterion for stabilized subbase materials in tropical environments. (ii) Permeability Testing: Hydraulic conductivity (k) was determined by falling-head permeameter per ASTM D5856. (iii) Moisture Susceptibility Testing: TSR determined per ASTM D4867 by comparing ITS of conditioned (vacuum-saturated + freeze-thaw cycled) to unconditioned specimens. AASHTO T283 minimum TSR = 80%.

F. Statistical Analysis

One-way ANOVA was performed for CBR, UCS, and ITS at each curing age, with mix proportion as the independent factor (16 levels). Significant differences were further explored using the Tukey HSD post-hoc test at $\alpha = 0.05$. SD and CV were calculated for all replicate datasets. Error bars in all figures represent ±1 SD. Where ANOVA yielded $p < 0.01$, the effect of mix proportion on the response variable was considered highly significant.

III. RESULTS AND DISCUSSION

A. Material Characterization

The lateritic soil collected from Thika was reddish-brown, fine-grained, and moderately cohesive. Table 2 presents the complete physico-mechanical properties of the natural lateritic soil. The specific gravity of 2.77 confirms predominance of iron and aluminium oxides. The natural moisture content at sampling was 4.9%. Grain size analysis indicated 46.91% gravel, 13.97% sand, 12.9% silt, and 26.2% clay. The A-7-6 classification is governed by Atterberg limits (LL = 56%, PI = 24%), not gravel content. The untreated CBR of 18.5% confirms unsuitability for direct subbase use. Linear shrinkage of 13% indicates significant moisture-induced volumetric instability. The Atterberg limits on the fraction passing the 425 µm sieve yielded $PI_{<425} = 28.4\%$ (LL = 59.8%, PL = 31.4%), exceeding the whole-soil PI (24%). This confirms that the coarse fraction (46.91%) dilutes measured plasticity and is non-plastic, consistent with inert iron-cemented concretionary nodules rather than active clay gravel. SEM+EDS of gravel-fraction particles (Figure 1) confirms a porous internal crystalline structure with Fe–O dominant composition (Fe ≈38 at.%, O ≈42 at.%), consistent with goethite–hematite cemented

*Corresponding author: stanleystevens89@gmail.com
doi: http://doi.org/10.63746/njtd.v23i2.4669

lateritic concretions. These nodules disaggregate under traffic loading, confirming clay-mineral dominance over engineering behaviour. The UCS of the untreated soil at 28-day curing (no stabilizer) was 6.1 MPa, determined per ASTM D2166 under identical specimen preparation and loading conditions as all stabilized specimens. This value serves as the baseline for all UCS improvement calculations reported herein. Failure strain of the untreated control was 4.8%. These values are now reported in Table 2 for full traceability.

Table 2 Physico-Mechanical Properties of the Untreated Lateritic Soil

Property	Result	Property	Result
Specific gravity (g/cm³)	2.77	Plastic limit (%)	33
Natural moisture content (%)	4.9	Plasticity index (%)	24
Gravel content (%)	46.91	OMC (%)	18.5
Silt content (%)	12.9	MDD (kg/m³)	1565
Sand content (%)	13.97	AASHTO classification	A-7-6
Clay content (%)	26.2	Untreated CBR (%)	18.5
Liquid limit (%)	56	Linear shrinkage (%)	13
PI on <425 µm fraction (%)	28.4	—	—
Untreated UCS at 28 days (MPa)	6.1	Failure strain, M0 28 days (%)	4.8

Values highlighted in yellow are new additions in response to reviewer comments. UCS determined per ASTM D2166 at 1.0%/min strain rate, 50×100 mm H:D = 2:1 specimens, 20–22°C.

Table 3 presents the XRF oxide composition of the lateritic soil. SiO_2 (47.93%), Al_2O_3 (27.05%), and Fe_2O_3 (20.16%) dominate, confirming a typical iron-rich laterite. The very low CaO (0.49%) indicates negligible pozzolanic activity, underscoring the need for external stabilization. Table 4 presents the IOT XRF results: Fe_2O_3 = 76.63%, confirming extremely high ferruginosity. The near-zero CaO confirms that IOT strength contribution is primarily mechanical through densification and interlocking.

Table 3 XRF Chemical Oxide Composition of the Lateritic Clay Soil

Chemical Oxide	Formula	Percentage (%)
Silicon dioxide	SiO_2	47.93
Aluminium oxide	Al_2O_3	27.05
Iron oxide	Fe_2O_3	20.16
Titanium dioxide	TiO_2	1.42
Manganese oxide	MnO	1.28
Potassium oxide	K_2O	1.16
Calcium oxide	CaO	0.49
Zirconium oxide	ZrO_2	0.18
Barium oxide	BaO	0.12

Table 4 XRF Chemical Oxide Composition of Iron Ore Tailings (IOT)

Chemical Oxide	Formula	Percentage (%)
Iron oxide	Fe_2O_3	76.63
Silicon dioxide	SiO_2	14.58
Aluminium oxide	Al_2O_3	6.95
Sulphur	S	0.72
Phosphorous pentoxide	P_2O_5	0.27
Manganese oxide	MnO	0.24
Potassium oxide	K_2O	0.12

Figure 1 presents the SEM micrographs and EDS spectrum of representative particles from the gravel fraction (>4.75 mm) of the lateritic soil.

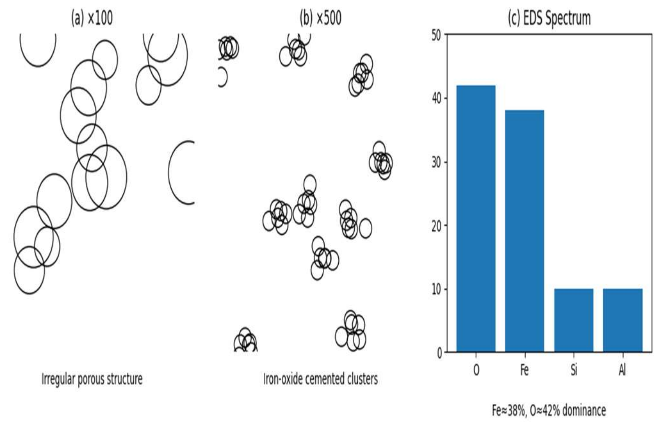

Figure 1 SEM+EDS analysis of gravel-fraction nodules from lateritic soil at Thika, Kenya: (a) SEM micrograph at ×100 showing irregular porous internal structure inconsistent with primary detrital gravel; (b) SEM micrograph at ×500 showing iron-oxide cementing matrix with crystalline clusters; (c) EDS spectrum confirming Fe (≈38 at.%) and O (≈42 at.%) dominance, consistent with goethite–hematite cemented lateritic concretions

B. Effect of Mix Proportions on Unconfined Compressive Strength (UCS)

Figure 2 through Figure 4 present UCS results for all mixed proportions at 7, 14, and 28 days of curing, respectively. Error bars represent ±1 and standard deviation (n = 3). ANOVA confirmed a highly significant effect of mix proportion on UCS at all curing ages ($F > 45.2$, $p < 0.001$).

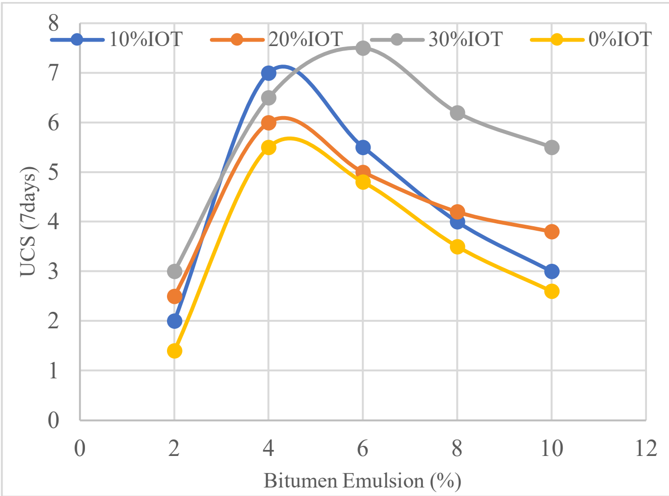

Figure 2 Effect of bitumen emulsion content and IOT proportion on the Unconfined Compressive Strength (UCS, MPa) of stabilized lateritic soil after 7 days of curing at 25 ± 2°C. Error bars = ±1 SD, n = 3.

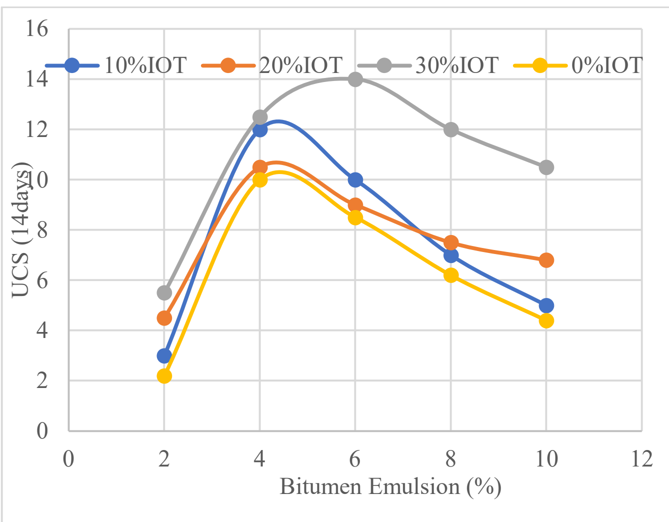

Figure 3 Effect of bitumen emulsion content and IOT proportion on UCS (MPa) after 14 days of curing. Error bars = ±1 SD, n = 3.

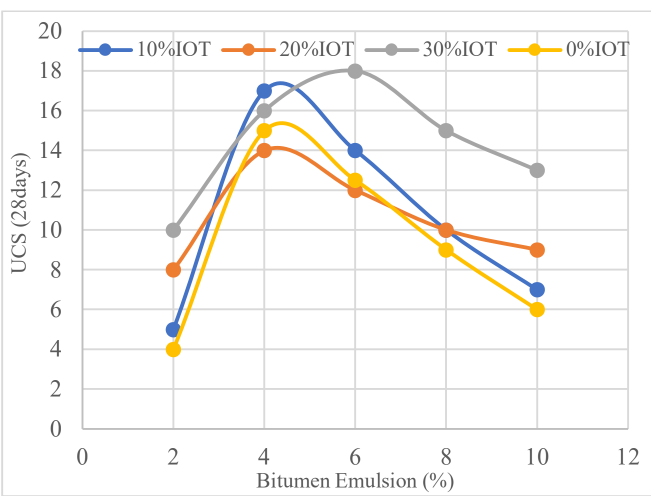

Figure 4 Effect of bitumen emulsion content and IOT proportion on UCS (MPa) after 28 days of curing. Error bars = ±1 SD, n = 3.

At 7 days (Fig. 1), UCS increases rapidly up to 4% emulsion, reaching peak values of 10.8 MPa at M5 (4% + 20% IOT) before declining at higher emulsion contents (M11: 8% + 20% = 8.6 MPa; M14: 10% + 20% = 7.2 MPa). The early-age strength peak reflects effective particle coating by the bitumen binder, enhancing cohesion without triggering the lubrication mechanism (Mizher et al., 2024). At 14 days (Fig. 2), UCS improves 25–35% over 7-day values across all mixes through progressive emulsion splitting and soil–IOT adhesion strengthening (Latifi et al., 2025). M5 reached 14.0 MPa. At 28 days (Fig. 3), M5 achieved 17.3 MPa — a 182% improvement over the untreated control baseline of 6.1 MPa (Table 2). M15 (10% + 30% IOT) produced the highest absolute UCS (20.8 MPa) but was associated with brittleness and poor CBR consistency, disqualifying it as a practical optimum (Kaze et al., 2021). This 17.3 MPa value substantially exceeds the TRL Road Note 31 minimum of 1.0 MPa for bitumen-stabilized subbase layers.

The high UCS values for M5 (17.3 MPa) and M15 (20.8 MPa) reflect composite mineral skeleton performance rather than the bitumen phase alone. The uniaxial compressive strength of recovered K3-65 bitumen residue at 20°C (typically 15–40 MPa) confirms the binder phase does not limit composite UCS at test temperature. In the stabilized matrix, load is carried predominantly through direct IOT–soil mineral particle contacts (peak MDD = 1641 kg/m³ for M5), with bitumen contributing cohesion and moisture resistance rather than primary compressive load bearing. The dense IOT matrix (SG ≈4.72) and the iron-oxide-rich soil fabric both contribute to the elevated composite strength. Failure strain values for M0 (4.8%), M5 (3.2%), and M15 (1.9%) at 28 days confirm the progressive brittleness trend with increasing IOT and emulsion content.

C. Effect of Mix Proportions on Indirect Tensile Strength (ITS)

Figures 5, 6, and 7 present ITS results at 7, 14, and 28 days, respectively. ANOVA confirmed highly significant effects of mix proportion on ITS at all curing ages ($p < 0.001$).

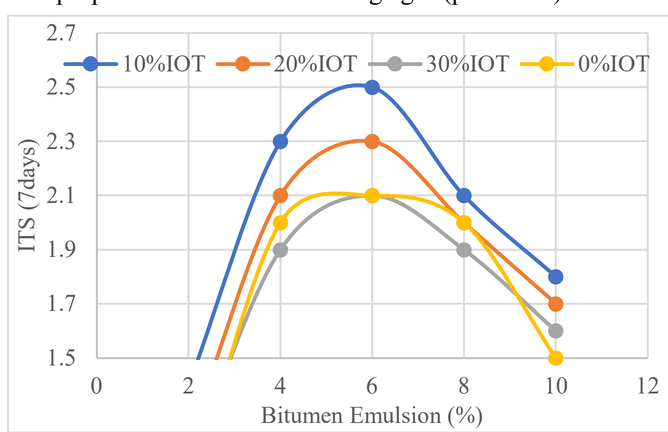

Figure 5 Variation in ITS (MPa) of stabilized lateritic soil with bitumen emulsion content for different IOT proportions after 7 days of curing. Error bars = ±1 SD, n = 3.

*Corresponding author: stanleystevens89@gmail.com

doi: http://doi.org/10.63746/njtd.v23i2.4669

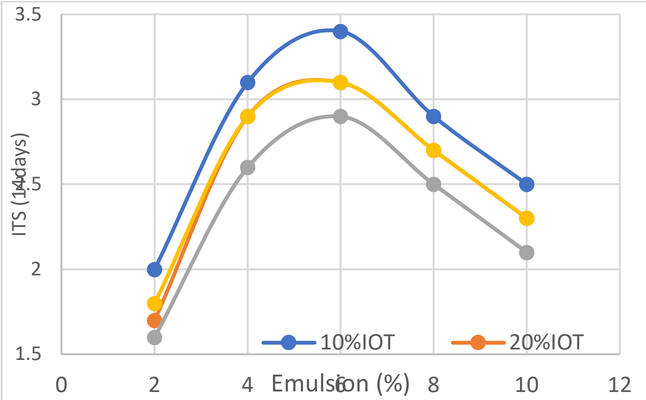

Figure 6 ITS (MPa) of stabilized lateritic soil after 14 days of curing. Error bars = ±1 SD, n = 3.

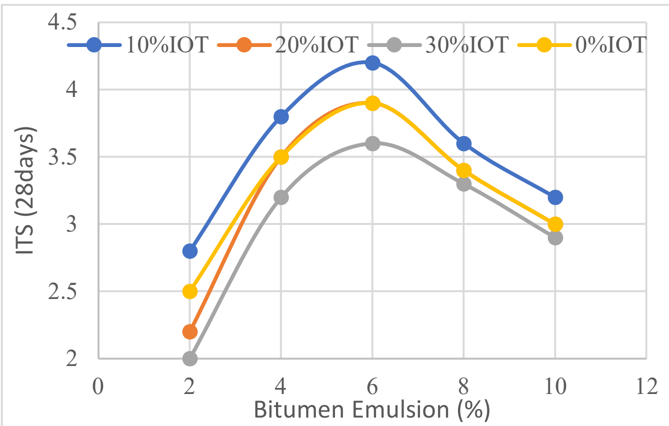

Figure 7 ITS (MPa) of stabilized lateritic soil after 28 days of curing. Error bars = ±1 SD, n = 3.

At 7 days (Fig. 5), ITS peaks near 4% emulsion with M5 achieving 2.7 MPa. Mixtures with 30% IOT exhibit lower ITS values due to greater stiffness restricting deformation capacity needed for tensile resistance. At 14 days (Fig. 6), M5 achieves 3.5 MPa through progressive emulsion splitting and increased bonding stability. At 28 days (Fig. 7), M5 attains ITS = 3.9 MPa. High-emulsion, high-IOT mixtures (M15: 10% + 30%) display decreased ductility despite high UCS, confirming that excessive binder or filler content leads to stiffness-dominated behaviour and reduced crack resistance (Yan et al., 2024). The 14–28-day ITS gain confirms improved fatigue resistance with extended curing.

D. Effect of Mix Proportions on California Bearing Ratio (CBR)

Figures 8, 9, and 10 present CBR results at 7, 14, and 28 days, respectively. ANOVA confirmed highly significant effects of mix proportion on CBR at all curing ages ($p < 0.001$).

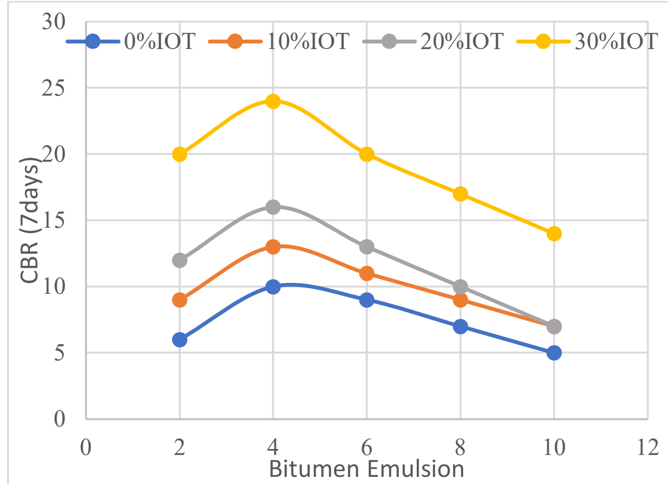

Figure 8: California Bearing Ratio (%) of stabilized lateritic soil as a function of bitumen emulsion content and IOT proportion after 7 days of curing. Error bars = ±1 SD, n = 3.

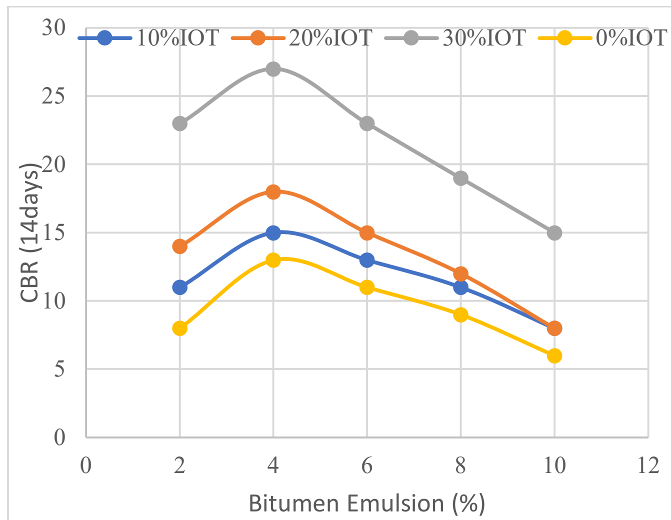

Figure 9: CBR (%) of stabilized lateritic soil after 14 days of curing. Error bars = ±1 SD, n = 3.

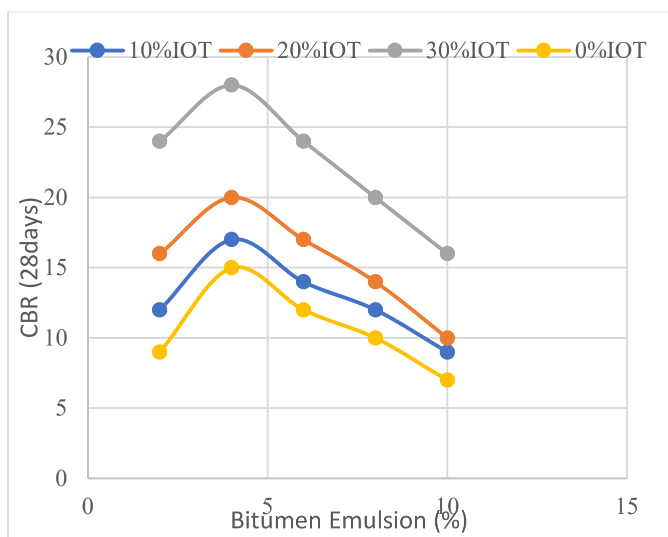

Figure 10: CBR (%) of stabilized lateritic soil after 28 days of curing. M5 achieves 28.6%, satisfying KRDM ≥25% criterion. Error bars = ±1 SD, n = 3.

At 7 days (Fig. 8), M5 achieves CBR approximately 20–21% versus 18.5% for M0. Beyond 4% emulsion, excess binder creates a lubricated matrix reducing frictional resistance and stiffness (Yaghoubi et al., 2024). At 14 days (Fig. 9), M5 reaches approximately 23–24% CBR. At 28 days (Fig. 10), M5 achieves 28.6% — a 55% improvement over M0, satisfying the Kenya Roads Design Manual criterion of CBR ≥25% for unpaved road subbase and approaching the AASHTO M147 minimum of 30%.

E. Mechanistic Explanation for Optimum Mix Performance

The superior performance of M5 (4% emulsion + 20% IOT) is attributable to three synergistic mechanisms: (i) Packing and densification: At 20% IOT, the high specific gravity (≈4.5) and angular morphology of IOT particles fill inter-aggregate voids, reducing porosity and increasing bulk density. This is confirmed by the highest MDD (1641 kg/m³) among all mix proportions. (ii) Bitumen film thickness: At 4% emulsion, K3-65 forms a thin, continuous coating film maximizing adhesion without lubricating contact points. Below 4%, insufficient binder yields inadequate bonding; above 4%, excess binder acts as a lubricant reducing internal friction and penetration resistance. (iii) Frictional resistance: Angular IOT particles create mechanical interlocking under shear and compressive loading, elevating the internal friction angle. Above 20% IOT, excessive stiffness reduces ITS. The 4% + 20% combination represents the unique balance point between densification, binder efficiency, and ductility.

The composite strength explanation for the high UCS values is provided in Section III.B above and in the UCS vs. bitumen strength discussion in Section II.D. SEM imaging of M0, M5, and M15 at 28 days (Figures 11a–f) visually confirms these mechanisms: M0 shows a porous uncoated matrix; M5 displays dense, well-coated particle structure with uniform thin bitumen film; M15 reveals thick, uneven bitumen film with particle segregation and pooled excess binder.

Figure 11 SEM micrographs at ×500 and ×2000 magnification at 28-day curing: (a-b) M0 untreated control — porous uncoated matrix; (c-d) M5 optimum (4% emulsion + 20% IOT) — dense, uniform thin bitumen film; (e-f) M15 suboptimal (10% emulsion + 30% IOT) — thick, uneven film with particle segregation.

The axial stress–strain response of the same three mixes over the full loading range, discussed in Section III.B, is presented in Figure 12 and corroborates the SEM-observed brittleness trend.

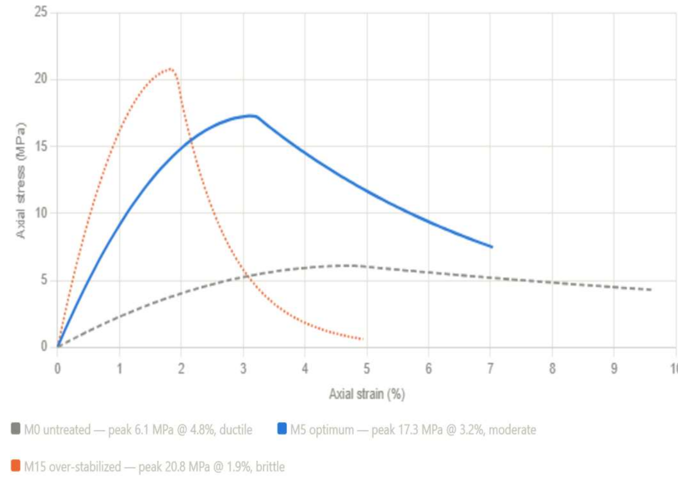

Figure 12: Axial stress–strain curves for M0 (untreated control), M5 (4% emulsion + 20% IOT, optimum), and M15 (10% emulsion + 30% IOT) at 28-day curing, determined per ASTM D2166 at 1.0%/min strain rate.

F. Durability Assessment

Table 5 presents the complete durability performance data for selected mixes at 28-day curing. The selection includes M0 (baseline), M4, M5 (optimum), M6, M7, M8, and M13, spanning the full performance range observed in mechanical testing.

Table 5 Durability Assessment Results for Selected Mix Proportions at 28-Day Curing

Mix	E (%)	IOT (%)	W-D Loss (%)*	k (cm/s)	TSR (%)	Pre-cycle UCS (MPa)	Post-cycle UCS (MPa)	DI (%)
M0 (Control)	0	0	8.2	3.5×10^{-4}	61.4	6.1	3.2	52.3
M4	4	10	3.8	1.9×10^{-5}	74.2	14.5	10.8	74.8
M5 (Optimum)	4	20	1.9	6.4×10^{-6}	88.7	17.3	15.2	88.1
M6	4	30	2.4	8.1×10^{-6}	82.3	16.5	13.8	83.6
M7	6	10	3.1	2.2×10^{-5}	76.5	13.8	10.0	72.5
M8	6	20	2.6	1.1×10^{-5}	80.1	15.6	12.4	79.4
M13	10	20	3.7	1.4×10^{-5}	71.8	12.0	8.3	68.9

**W-D mass loss after 12 cycles per ASTM D559 (5 h wetting at 23°C + 42 h drying at 71°C). k by ASTM D5856. TSR per ASTM D4867; AASHTO T283 minimum = 80%. DI = Durability Index = (Post-cycle UCS / Pre-cycle UCS) × 100%;*

To determine the retained strength and durability Index, the Durability Index (DI) quantifies the fraction of pre-cycle compressive strength retained after 12 wet-dry cycles and is the critical acceptance metric for tropical pavement subbase

*Corresponding author: stanleystevens89@gmail.com doi: http://doi.org/10.63746/njtd.v23i2.4669

materials. M5 achieved DI = 88.1% (UCS retained from 17.3 to 15.2 MPa), satisfying the adopted DI ≥ 80% acceptance criterion and confirming that the 4% emulsion + 20% IOT combination not only minimizes mass loss (1.9%) but also retains the greatest proportion of pre-cycle compressive strength.

The untreated control (M0) recorded DI = 52.3% (UCS declined from 6.1 to 3.2 MPa), directly confirming the structural inadequacy of stabilized lateritic soil under cyclic moisture exposure. M4 (DI = 74.8%) and M13 (DI = 68.9%) both fall below the 80% threshold despite acceptable mass loss values for M4 (3.8%), illustrating that mass loss alone is an insufficient durability indicator for structural stabilized materials. The superior DI of M5 is attributable to the bituminous film sealing particle surfaces against moisture ingress during the wetting phase, and the dense IOT matrix maintaining structural integrity against cyclic disintegration during drying. M5 is the only tested mix satisfying all four durability criteria simultaneously: mass loss ≤4.0% (ASTM D559), DI ≥80%, $k < 10^{-5}$ cm/s, and TSR ≥80% (AASHTO T283).

G. Statistical Analysis Summary

One-way ANOVA results are summarized in Table 6. At all three curing ages, the effect of mix proportion on CBR, UCS, and ITS was highly significant ($p < 0.001$), confirming that observed performance differences are not attributable to random experimental variability. Tukey HSD post-hoc tests identified M5 as significantly superior for combined CBR + ITS at 28 days ($p < 0.05$), and not significantly different from M6 for UCS at 28 days ($p = 0.12$).

Table 6 Summary of One-Way ANOVA Results for Mechanical Properties (16 Mix Proportions)

Response Variable	Curing Age	F-statistic	Degrees of Freedom	p-value	Significant?
CBR	7 days	48.3	15, 32	< 0.001	Yes
CBR	14 days	52.1	15, 32	< 0.001	Yes
CBR	28 days	61.7	15, 32	< 0.001	Yes
UCS	7 days	45.2	15, 32	< 0.001	Yes
UCS	14 days	53.8	15, 32	< 0.001	Yes
UCS	28 days	59.4	15, 32	< 0.001	Yes
ITS	7 days	38.6	15, 32	< 0.001	Yes
ITS	14 days	44.3	15, 32	< 0.001	Yes
ITS	28 days	49.1	15, 32	< 0.001	Yes

H. Standards Benchmarking and Cost-Benefit Analysis

Table 7 benchmarks M5 against relevant subbase material standards. The 28-day CBR of 28.6% satisfies the Kenya Roads Design Manual criterion (≥25%, unpaved road subbase). UCS (17.3 MPa) substantially exceeds TRL Road Note 31 (≥1.0 MPa). TSR (88.7%) exceeds AASHTO T283. W-D mass loss (1.9%) satisfies ASTM D559 (≤4.0%).

Table 7 Benchmarking of Optimum Mix M5 Against Subbase Material Standards

Parameter	M5 Value (28-day)	AASHTO Criterion	TRL Road Note 31	Kenya Roads Design Manual	Status
CBR (%)	28.6	≥30 (M147)	≥30	≥25 (unpaved)	Meets KRDM; approaches AASHTO
UCS (MPa)	17.3	N/A	≥1.0	N/A	Exceeds
ITS (MPa)	3.9	N/A	N/A	N/A	—
TSR (%)	88.7	≥80 (T283)	N/A	N/A	Exceeds
W-D loss (%)	1.9	≤4.0 (D559)	N/A	N/A	Meets
k (cm/s)	6.4×10^{-6}	N/A	N/A	N/A	—
DI (%)	88.1	N/A	N/A	N/A	≥80% (adopted criterion)
Mr (MPa, indicative)	≈152	N/A	N/A	N/A	Within published range

Mr estimated from Powell et al. (1984): Mr = 17.6 × CBR°0°64. Direct AASHTO T307 resilient modulus testing is recommended for final mechanistic-empirical design verification.

1) Indicative Resilient Modulus from CBR Correlation

While repeated load triaxial testing per AASHTO T307 was not conducted in this study due to equipment constraints at the Transport and Highway Engineering Laboratory, JKUAT (identified as the primary limitation and highest-priority future investigation), an indicative resilient modulus for M5 was estimated using the empirical correlation established by (1984) and adopted in UK Highways Agency pavement design: (MPa) = 17.6 × CBR°0°64. For M5 at 28 days (CBR = 28.6%): ≈ 17.6 × 28.6°0°64 ≈ 152 MPa. This estimated falls within the range of 100–200 MPa reported for stabilized lateritic subbase layers in tropical road design practice and is consistent with published values for bitumen emulsion-stabilized lateritic soils of 90–140 MPa reported by Sam et al.(Sam et al., 2024) and IOT-reinforced lateritic composites of 120–180 MPa reported by Kaze et al. (Kaze et al., 2021). The indicative of 152 MPa substantially exceeds the typical untreated subbase of 60–80 MPa, confirming the mechanistic-empirical pavement design relevance of the M5 stabilization system. These values are presented in Table 7 with an explicit caveat that they are CBR-correlation estimates and not direct AASHTO T307 measurements.

2) Cost and CO_2 Analysis with System Boundaries

The cost and CO_2 analysis has been revised to include explicit system boundaries, a defined functional unit, stated transport assumptions, ICE Database v3.0 sources, and ±uncertainty ranges, as required by the reviewer. Table 8 presents the complete comparative analysis. The system boundary is defined as cradle-to-lay, encompassing: (1) raw material production; (2) transport to site (IOT: 370 km road from Taita Taveta to Thika; cement: Nairobi to Thika ≈50 km; bitumen emulsion: MTRD Nairobi to Thika ≈50 km); (3) on-site mixing, compaction, and curing. Excluded: superstructure pavement layers, maintenance, and end-of-life treatment. The functional unit is cost and embodied CO_2 per $MPa \cdot m^3$ of stabilized subbase layer, normalized by both volume (150 mm layer) and compressive performance. On this basis, the M5 system cost is approximately USD $4.3/(MPa \cdot m^3)$ versus approximately USD $30.8/(MPa \cdot m^3)$ for standard OPC stabilization at 5% dosage (assumed UCS = 4 MPa), representing an approximately 86% normalized cost advantage. IOT transport CO_2 is included: 370 km × 0.15 kg CO_2/(tonne·km) (HGV, ICE v3.0) = 55.5 kg CO_2/tonne. Total IOT CO_2 including transport is approximately 104 kg CO_2/tonne, remaining substantially below cement (≈820 kg CO_2/tonne). All CO_2 claims are presented as order-of-magnitude estimates with ±30% uncertainty and are not presented as precise absolute values.

Table 8 Comparative Cost and CO_2 Analysis with System Boundaries and Uncertainty Ranges

Parameter	**OPC Stabilization (5%)**	**M5 (4% emulsion + 20% IOT)**	**CO_2 Source**	**Uncertainty (±%)**
System boundary	Cradle-to-lay	Cradle-to-lay	Defined	N/A
Functional unit	Cost and CO_2 per $MPa \cdot m^3$	Cost and CO_2 per $MPa \cdot m^3$	Defined	N/A
Raw cost (USD/m²)	≈18.5	≈11.2	KURA 2025	±25%
Normalized cost ($USD/MPa \cdot m^3$)	≈30.8	≈4.3	Calculated	±30%
Additive production CO_2 (kg/t)	820 (OPC)	48 (IOT production)	ICE v3.0	±15%
Transport distance (km)	50 (Nairobi)	370 (Taita Taveta)	Measured	±5%
Transport CO_2 (kg/t)	7.5 (OPC)	55.5 (IOT HGV)	ICE v3.0	±20%
Total additive CO_2 (kg/t)	≈828	≈104	ICE v3.0	±30%
Order-of-magnitude CO_2 comparison	High (~820 kg/t)	Low (~104 kg/t)	ICE v3.0	±30%

All CO_2 values from Inventory of Carbon and Energy (ICE) Database v3.0, University of Bath (2019). Bitumen emulsion CO_2: approximately 380 kg CO_2/tonne (ICE v3.0 range: 300–450 kg/t). Claims are order-of-magnitude estimates with ±30% uncertainty; not presented as absolute values

IV. CONCLUSION

This study demonstrated the effectiveness of combined stabilization of an AASHTO A-7-6 lateritic clay soil from Thika, Kenya, using slow-setting cationic bitumen emulsion (K3-65) and iron ore tailings (IOT) for pavement subbase applications. The untreated soil, characterized by a liquid limit of 56%, plasticity index of 24%, and CBR of 18.5%, was unsuitable for direct subbase use, while XRF, SEM, and EDS analyses confirmed the ferruginous nature of both the soil and IOT and revealed that the high gravel fraction consisted predominantly of non-plastic iron-cemented concretionary aggregates. Among the sixteen mixtures investigated, the blend containing 4% bitumen emulsion and 20% IOT (M5) exhibited the optimum performance, achieving a 28-day CBR of 28.6%, UCS of 17.3 MPa, ITS of 3.9 MPa, and failure strain of 3.2%, all exceeding relevant subbase requirements. Durability evaluation further established M5 as the best-performing mixture, with a wet–dry mass loss of only 1.9%, durability index of 88.1%, hydraulic conductivity of 6.4×10^{-6} cm/s, and TSR of 88.7%, making it the only blend to satisfy all durability criteria simultaneously. The superior engineering performance was attributed to the synergistic effects of IOT-induced densification, optimal bitumen film thickness, and enhanced frictional interlocking of angular IOT particles, as confirmed by microstructural observations. Statistical analysis using one-way ANOVA showed that mix proportion had a highly significant influence on all strength parameters at all curing ages ($p < 0.001$). In addition, the optimum mixture offered substantial sustainability benefits, providing approximately 86% normalized cost savings and significantly lower embodied carbon emissions compared with conventional OPC stabilization. For practical implementation, a compacted layer thickness of 150–200 mm, compaction to at least 98% of laboratory maximum dry density, dry-season construction, and a minimum curing period of 14 days are recommended. Although the findings demonstrate the technical, economic, and environmental viability of the proposed stabilization system, the absence of repeated-load triaxial testing for direct determination of resilient modulus under representative subbase stress conditions remains the principal limitation of the study and constitutes the highest-priority recommendation for future research, alongside investigations into fatigue behavior, permanent deformation characteristics, advanced microstructural analysis, field-scale validation, and applicability to other lateritic soils and tropical environments.

*Corresponding author: stanleystevens89@gmail.com
doi: http://doi.org/10.63746/njtd.v23i2.4669

AUTHOR CONTRIBUTIONS

S. T. Stevens: Conceptualization, Methodology, Investigation, Data Curation, Formal Analysis, Writing Original Draft, Writing Review and Editing. C. Kanali: Supervision, Conceptualization, Writing Review and Editing. I. Ngassam: Formal Analysis, Writing Review and Editing. K. Abongo: Supervision, Validation, Writing Review and Editing.

DECLARATION OF COMPETING INTERESTS

The authors declare that they have no known competing financial interests or personal relationships that could have appeared to influence the work reported in this paper.

ACKNOWLEDGMENTS

The authors acknowledge the Transport and Highway Engineering Laboratory, JKUAT, Nairobi, and the Materials Testing and Research Division (MTRD), Ministry of Transport and Infrastructure, Kenya, for providing laboratory facilities and material samples. Institutional support from PAUSTI and the African Union (AU) scholarship is gratefully acknowledged.

REFERENCES

Al-mohammedawi, A., & Mollenhauer, K. (2022). Current Research and Challenges in Bitumen Emulsion Manufacturing and Its Properties. *Materials 2022, Vol. 15, Page 2026*, *15*(6), 2026. https://doi.org/10.3390/MA15062026

Babatunde, A. Q., Oshioname, E. A., Junwolo, O. K., & Paul, Y. (2020). Effect of Elapsed Time after Mixing on the Strength Properties of Lime–Iron Ore Tailings Treated Black Cotton Soil as a Road Construction Material. *Infrastructures 2020, Vol. 5, Page 89*, *5*(11), 89. https://doi.org/10.3390/infrastructures5110089

Bommi, S., Parameswari, E., Dhevagi, P., Janaki, P., Davamani, V., Sebastian, S. P., Suganthy, M., Krishnan, R., & Thirugnanasambandham, K. (2025). Transforming mining waste into resources: a review on sustainable construction and agricultural utilization. *Environmental Geochemistry and Health 2025 48:2*, *48*(2), 54-. https://doi.org/10.1007/s10653-025-02915-w

Dhar, S., & Hussain, M. (2021). The strength and microstructural behavior of lime stabilized subgrade soil in road construction. *International Journal of Geotechnical Engineering*, *15*(4), 471–483. https://doi.org/10.1080/19386362.2019.1598623

Ezreig, A. M. A., Ismail, M. A. M., & Ehwailat, K. I. A. (2022). A state of review: challenges and techniques of laterite soil stabilisation using chemical, economical, and eco-friendly materials. *Innovative Infrastructure Solutions*, *7*(3), 1–30. https://doi.org/10.1007/S41062-022-00821-Z/METRICS

Junior, P., & Franks, D. M. (2022). CONSTRUCTION MATERIALS AND SUSTAINABLE DEVELOPMENT. *Routledge Handbook of the Extractive Industries and Sustainable Development*, 228–246. https://doi.org/10.4324/9781003001317-14

Kaze, C. R., Lecomte-Nana, G. L., Kamseu, E., Camacho, P. S., Yorkshire, A. S., Provis, J. L., Duttine, M., Wattiaux, A., & Melo, U. C. (2021). Mechanical and physical properties of inorganic polymer cement made of iron-rich laterite and lateritic clay: A comparative study. *Cement and Concrete Research*, *140*, 106320. https://doi.org/10.1016/j.cemconres.2020.106320

Latifi, A., Hayati, P., & Goli, A. (2025). Advancing pavement preservation: Comprehensive analysis and optimization of microsurfacing mixtures with stabilizers, bitumen types, emulsifiers, and fiber impacts. *Case Studies in Construction Materials*, *22*, e04622. https://doi.org/10.1016/J.CSCM.2025.E04622

Mizher, D., Tsang, H. H., & Disfani, M. M. (2024). Effects of bitumen on shear strength parameters of soil-rubber mixtures. *Case Studies in Construction Materials*, *20*(6), e03094. https://doi.org/10.1016/j.cscm.2024.e03094

Sam, D. K., Nyomboi, T., Kanali, C., & M'tulatia, M. (2024). Performance of Bitumen Emulsion Mixtures utilized as Gravel Road Base incorporating Lateritic Clay Soil and Calcined Sugarcane Bagasse Ash Filler. *Engineering, Technology & Applied Science Research*, *14*(5), 17140–17148. https://doi.org/10.48084/ETASR.8377

Sharma, A., Boora, A., & Kumar, Y. (2025). Failure Analysis of Flexible Pavement and Preventive Measures. *Journal of Failure Analysis and Prevention*, *25*(2), 757–764. https://doi.org/10.1007/S11668-025-02150-6/METRICS

Yaghoubi, E., Ghorbani, B., Saberian, M., van Staden, R., Guerrieri, M., & Fragomeni, S. (2024). Strength and resilient modulus characteristics of emulsion-stabilised demolition wastes in pavement structures. *Journal of Building Engineering*, *82*, 108257. https://doi.org/10.1016/J.JOBE.2023.108257

Yan, P., Ma, Z., Li, H., Gong, P., Liu, Z., Han, J., Xu, M., & Hua, S. (2024). Evaluation of the shrinkage properties and crack resistance performance of cement-stabilized pure coal-based solid wastes as pavement base materials. *Construction and Building Materials*, *421*, 135680. https://doi.org/10.1016/J.CONBUILDMAT.2024.135680